NUMERICAL ANALYSIS OF TURBULENT FORCED CONVECTION IN A CHANNEL WITH FLAT AND DIAMOND-SHAPED BAFFLES OF DIFFERENT HEIGHTS

ANALYSE NUMERIQUE DE LA CONVECTION FORCEE TURBULENTE DANS UN CANAL MUNI DES CHICANES PLANES ET LOSANGES DE DIFFERENTES HAUTEURS

Y. MENNI, A. AZZI, CH. ZIDANI

Research Unit of Materials and Renewable Energies (URMER),
Department of Physics, Faculty of Sciences, Abou Bekr Belkaid University, Tlemcen BP 119-13000-Tlemcen, Republic of Algeria
Youtifa_URMER.Physic@hotmail.fr/menniyounes@gmail.com, a_azzi@mail.univ-tlemcen.dz, czidani10@yahoo.fr

ABSTRACT

Forced-convection airflow characteristics were examined for a constant property fluid flowing turbulently through a rectangular channel with staggered, transverse baffles and a constant temperature along both walls. Two models of baffles were considered in this study, flat and/or diamond-shaped baffles. Computations were carried out in the steady-state for different baffle heights. The fluid flow and heat transfer characteristics are simulated using software CFD ANSYS FLUENT 14.0. The influence of the diamond shape on the convective heat transfer phenomenon is shown and this in comparing the results of this type with those of the flat baffle. The computational results reveal essentially, that the shape of the obstacle can alter substantially the airflow and heat transfer behaviors. In addition, it is shown that an increase in the deflector height cause a substantial increase in the fluid velocity and heat transfer but the friction loss is also very significant for both cases studied.

KEYWORDS: Turbulent forced convection, diamond baffle, flat baffle, rectangular channel, CFD.

RESUME

Des caractéristiques d'écoulement d'air en convection forcée sont examinées pour un fluide à propriétés constantes qui s'écoule en régime turbulent à travers une conduite rectangulaire avec des chicanes transverses et étagées et une temperature le long des parois. Deux modèles de chicanes ont été considérés dans cette étude, chicanes rectangulaire plane et/ou losange. Des calculs sont menés dans l'état stationnaire pour différents hauteurs d'obstacle. Les caractéristiques d'écoulement et de transfert thermiques sont simulées en utilisant le logiciel CFD ANSYS FLUENT 14.0. L'influence de la forme losange sur le phénomène de transfer de chaleur convectif est illustrée et cela, en comparant les résultats obtenus pour les deux modèles de chicanes. Les résultats computationnels révèlent essentiellement que la forme d'obstacle peut modifier substantiellement les comportements d'écoulement d'air et de transfer thermiques. En outre, il est démontré que l'augmentation de la hauteur de déflecteur provoque une augmentation substantielle de la vitesse de fluide et du transfert de chaleur, mais la perte de charge est également très importante dans les deux cas étudiés.

MOTS CLES: Convection forcée turbulente, chicane losange, Chicane plane, canal rectangulaire, CFD.

1 INTRODUCTION

Improvement of heat transfer in thermal devices such as heat exchangers and electronic equipments became an important factor in industry. For this purpose, various techniques have been proposed as the use of treated surfaces, rough surfaces, extended surfaces, surface vibration, fluid vibration, jet impingement, staggered or in-line baffles, flat or shaped baffles, vertical or inclined baffles, solid or porous baffles, fins, blocks, corrugated channel, coiled tubes, twisted tape inserts, discontinuous crossed ribs and grooves. Most of these enhancement techniques are based on the baffle arrangement. Use of heat transfer enhancement techniques lead to increase in heat

transfer coefficient but at the cost of increase in pressure drop.

An extensive experimental studies of turbulent heat transfer past baffles in heat exchangers has been performed by various authors. Karwa et al. (2005) where conducted an experimental work on study of heat transfer and friction in rectangular ducts with baffles (solid or perforated) attached to one of the broad walls. The Reynolds number of the study ranges from 2850 to 11500. The baffled wall of the duct is uniformly heated while the remaining three walls are insulated. These boundary conditions correspond closely to those found in solar air heaters. Over the range of the study, the Nusselt number for the solid baffles is higher than that for the smooth duct, while for the perforated baffles. The friction factor for the solid baffles is found to be 9.6-11.1 times of the smooth duct, which decreased significantly for the perforated baffles with the increase in the open area ratio. Performance comparison with the smooth duct at equal pumping power shows that the baffles with the highest open area ratio give the best performance. Another experimental study conducted by Wilfried et al. (1994). These authors examined experimentally turbulent flows throughout tubular heat exchangers. The investigators focused on the impact of the baffles on heat transfer, and the geometrical properties of the heat-exchanger on the overall thermal efficiency.

Kang-Hoon et al. (2003) have experimentally determined the mean heat transfer coefficients in a rectangular channel with porous obstacles. One important result from this work is that the use of baffles improved the thermal efficiency by 300 %, compared with the case in which no baffles were used. Thermal and hydrodynamic parameters were examined numerically and experimentally by Yong-Gang Lei et al. (2008) for a flow passing through a channel with only one helicoidal baffle. A comparative study between three different channels was conducted by the investigators. In the first case, a channel without any baffles was examined. In the second case, the same channel with only one helicoidal baffle was examined. In the third case, the same channel with two helicoidal baffles was examined. Ahmet et al. (2006) examined the effect of the geometric parameters on the steady turbulent flow passing through a pipe with baffles. The effect of the orientation and the distance between nine baffles on the improvement of heat transfer was highlighted in this work. Another experimental investigation was carried out by Molki et al. (1989) to evaluate heat transfer and pressure losses in a rectangular channel with baffles. The authors concluded that baffles raise the pressure losses and the coefficient of heat transfer as well. An investigation of the thermo hydraulic parameters in a rectangular channel heated up by means of fins perforated to different heights is reported by Karwa and Maheshwari (2009). Demartini et al. (2004) investigated air flow through a rectangular channel with two plate baffles. A comprehensive analysis of the velocity profiles and pressure gradients was carried out in this work. While Demartini's approach used a rectangular channel with plate baffles, the question remains whether baffles of different shapes will achieve the same results.

The principal objective of the present study is to show the influence of solid baffle shape (i.e., flat and diamond-shaped) on the fluid flow and heat transfer characteristics when baffle height effect (h=0.04, 0.06, 0.08, 0.1, and 0.12, unit: m) is simultaneously present.

2 MATHEMATICAL FORMULATION

2.1 Problem Definition

The system of interest is a two-dimensional parallel plate channel with a baffle pair placed in a staggered array on the top and bottom channel walls as shown in Figure 1a and b. Two types of baffle shapes are designed for computational investigation; a first form is flat rectangular-shaped baffle (Fig. 1a), and a second baffle form is diamond (Fig. 1b).

To investigate a geometry effect of the interaction between both baffles, the baffle height (h) is varied in a range of h=0.04m to h=0.12m for each test run of calculations.

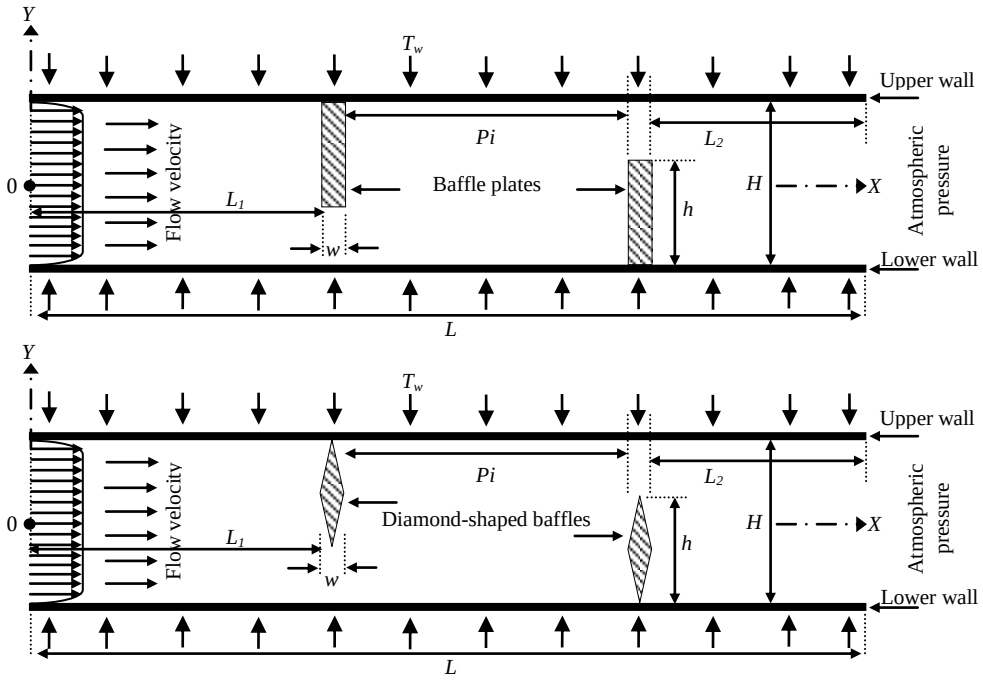

Figure 01: Schematic of the physical domain with: (a) flat rectangular, and (b) diamond-shaped baffles

The dimension of the constant temperature-surfaced rectangular test section mentioned above with top and bottom wall-mounted shaped baffles is the same as the baffled channel of Demartini et al. (2004) used for validation. In that study, the flow through a rectangular channel, where two baffle plates were placed in opposite walls, was studied. The geometry of the problem is a simplification of the geometry of baffle plates found in shell-and-tube heat exchangers. Tab. 1 indicates the important parameters of the system.

Table 01: Detail of Test Channel

Parameters (Unit : m)	***Value***
Channel length (L)	0.554
Channel height (H)	0.146
Hydraulic diameter (D_h)	0.167
Baffle height (h)	0.08
Baffle width (w)	0.01
Spacing (Pi)	0.142
Distance upstream of the first baffle (L_1)	0.218
Distance downstream of the second baffle (L_2)	0.174

Also, a typical diamond-shaped baffle pair with the same conditions is introduced for comparison. Commercial software FLUENT 6.3 (2006) is applied for the solution of the problem. The hydrodynamic boundary conditions are set according to the numerical and experimental work of Demartini et al. (2004) while the thermal boundary conditions are chosen according to the numerical work of Nasiruddin and Kamran Siddiqui (2007). A uniform one-dimensional velocity is applied as the hydraulic boundary condition at the inlet of the computational domain. The pressure at the inlet of the computational domain is set equal to the zero gauges. A constant temperature of 375K is applied on the entire wall of the computational domain as the thermal boundary condition. The temperature of the working fluid is set equal to 300K at the inlet of the channel. Besides, no-slip and impermeability boundary conditions are imposed at the channel wall as well as the baffles. In the channel outlet it is prescribed the atmospheric pressure.

2.2 Governing Equations

The numerical model for fluid flow and heat transfer in the channel was developed under the following assumptions:

- Steady two-dimensional fluid flow and heat transfer.
- The flow is turbulent and incompressible.
- Constant fluid properties.
- Body forces and viscous dissipation are ignored.
- Negligible radiation heat transfer.

Based on the above assumptions, the channel flow is governed by the continuity, the Navier-Stokes equations and the energy equation. The general transport equation can be written in the following conservative form:

$$\frac{\partial}{\partial x}(\rho u\phi)+\frac{\partial}{\partial y}(\rho v\phi)=\frac{\partial}{\partial x}\left[\Gamma_\phi\frac{\partial\phi}{\partial x}\right]+\frac{\partial}{\partial y}\left[\Gamma_\phi\frac{\partial\phi}{\partial y}\right]+S_\phi \qquad (1)$$

in which ϕ is a variable used to represent quantities such as velocity components u, v, turbulent kinetic energy k or turbulent energy dissipation rate ε, while the diffusion coefficient Γ_ϕ and the source term S_ϕ have specific values for the different conservation equations using the standard k-ε turbulence model (Launder and Spalding 1974) as
Continuity equation:

$$\phi = 1 \quad (2)$$

$$\Gamma_\phi = 0 \quad (3)$$

$$S_\phi = 0 \quad (4)$$

Momentum equation in X-direction:

$$\phi = u \quad (5)$$

$$\Gamma_\phi = \mu_e \quad (6)$$

$$S_\phi = -\frac{\partial p}{\partial x} + \frac{\partial}{\partial x}\left[\mu_e\left(\frac{\partial u}{\partial x}\right)\right] + \frac{\partial}{\partial y}\left[\mu_e\left(\frac{\partial v}{\partial x}\right)\right] \quad (7)$$

Momentum equation in Y-direction:

$$\phi = v \quad (8)$$

$$\Gamma_\phi = \mu_e \quad (9)$$

$$S_\phi = -\frac{\partial p}{\partial y} + \frac{\partial}{\partial x}\left[\mu_e\left(\frac{\partial u}{\partial y}\right)\right] + \frac{\partial}{\partial y}\left[\mu_e\left(\frac{\partial v}{\partial y}\right)\right] \quad (10)$$

Energy equation:

$$\phi = T \quad (11)$$

$$\Gamma_\phi = \frac{\mu_e}{\sigma_T} \quad (12)$$

$$S_\phi = 0 \quad (13)$$

k-turbulent kinetic energy equation:

$$\phi = \mathrm{k} \quad (14)$$

$$\Gamma_\phi = \mu_\lambda + \frac{\mu_t}{\sigma_k} \quad (15)$$

$$S_\phi = -\rho.\varepsilon + G \quad (16)$$

ε-turbulent dissipation rate equation:

$$\phi = \varepsilon \quad (17)$$

$$\Gamma_\phi = \mu_\lambda + \frac{\mu_t}{\sigma_\varepsilon} \quad (18)$$

$$S_\phi = \left(C_{1\varepsilon} f_1 G - C_{2\varepsilon} f_2 \rho.\varepsilon\right)\frac{\varepsilon}{k} \quad (19)$$

With:

$$G = \mu_t\left\{2.\left(\frac{\partial u}{\partial x}\right)^2 + 2.\left(\frac{\partial v}{\partial y}\right)^2 + \left(\frac{\partial v}{\partial x} + \frac{\partial u}{\partial y}\right)^2\right\} \quad (20)$$

$$\mu_e = \mu_\lambda + \mu_t \quad (21)$$

$$\mu_t = f_\mu \rho.C_\mu \frac{k^2}{\varepsilon} \quad (22)$$

C_μ=0.09; $C_{1\varepsilon}$=1.44; $C_{2\varepsilon}$=1.92; σ_k=1.0; σε=1.3; and σ_T=0.9 are the constants of the model (Launder and Spalding 1974).

The Reynolds number of the experiments (Endres and Möller 2001; Demartini et al. 2004), calculated with the hydraulic diameter, D_h of the channel and the reference velocity, $\overline{U}$ is Re=8.73×10^4, defined as :

$$\mathrm{Re} = \frac{\rho \overline{U} D_h}{\mu} \quad (23)$$

The friction factor, f is computed by pressure drop, ΔP across the length of the channel, L as:

$$f = \frac{(\Delta P / L) D_h}{\frac{1}{2}\rho \overline{U}^2} \quad (24)$$

The convective heat transfer is measured by local Nusselt number, Nu_x which can be written as:

$$Nu_x = \frac{h_x D_h}{\lambda_f} \quad (25)$$

The average Nusselt number, $\overline{Nu}$ can be obtained by :

$$\overline{Nu} = \frac{1}{L}\int Nu_x \partial x \qquad (26)$$

Where ρ presents the fluid density; μ is the dynamic viscosity of fluid, λ_f the thermal conductivity of fluid, and h_x is the local convective heat transfer coefficient.

3 NUMERICAL SOLUTION

The Commercial CFD software FLUENT 6.3 (2006) was used to simulate the fluid flow and heat transfer fields. As a part of the same package, a preprocessor Gambit 2.3 was used to generate the required mesh for the solver. Structured meshes with refinements near the solid boundary to resolve velocity, pressure, and temperature gradients. For the regions more distant from the walls, the mesh is uniform, as a tentative. The governing equations were discretized using the Finite Volume Method of Patankar (1980), using a two-dimensional formulation with the SIMPLE algorithm for pressure-velocity coupling (Patankar 1980). Considering the characteristics of the flow, the Quick-scheme was applied to the interpolations, while a second-order upwind scheme was used for the pressure terms. To control the update of the computed variables at each iteration; under-relaxation was varied between 0.3 and 1.0. The residual error less than 10-7 was set as the convergence criterion.

3.1 Mesh Analysis

The computational domain is resolved by regular Cartesian elements. A grid independence procedure was implemented by using the Richardson extrapolation technique over grids with different numbers of cells, 175×90 and 220×135. It is found that the variation in $\overline{Nu}$ and f values for the staggered flat baffle at h=0.08m and Re=8.73×10^4 is marginal when increasing the number of cells from 175×90 to 220×135. Hence, there is no such advantage in increasing the number of cells beyond this value.

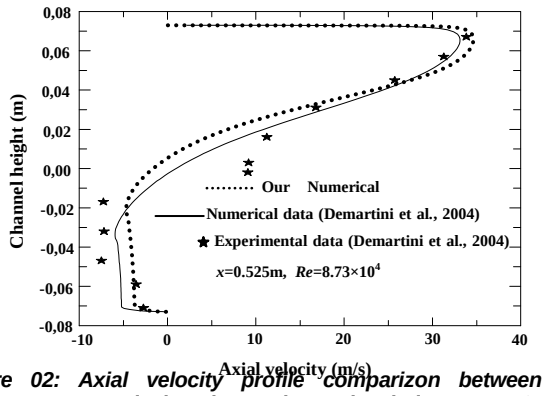

Figure 02: Axial velocity profile comparizon between the numerical and experimental solutions at x=0.525m for Re=8.73×10^4

Considering convergent time and solution precision, the grid system of 175×90 cells was adopted for the current computation.

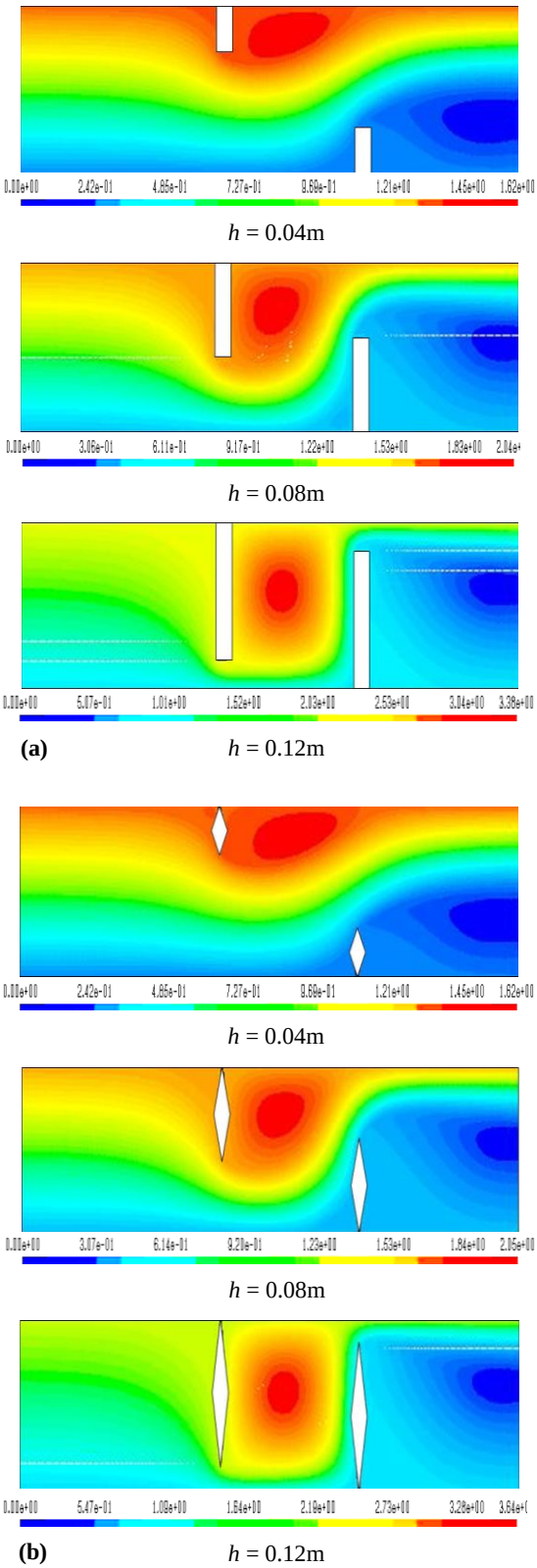

Figure 03: Effect of baffle height on streamlines (unit: Kg/s) for:
(a) flat and
(b) diamond baffles, Re=8.73×10^4

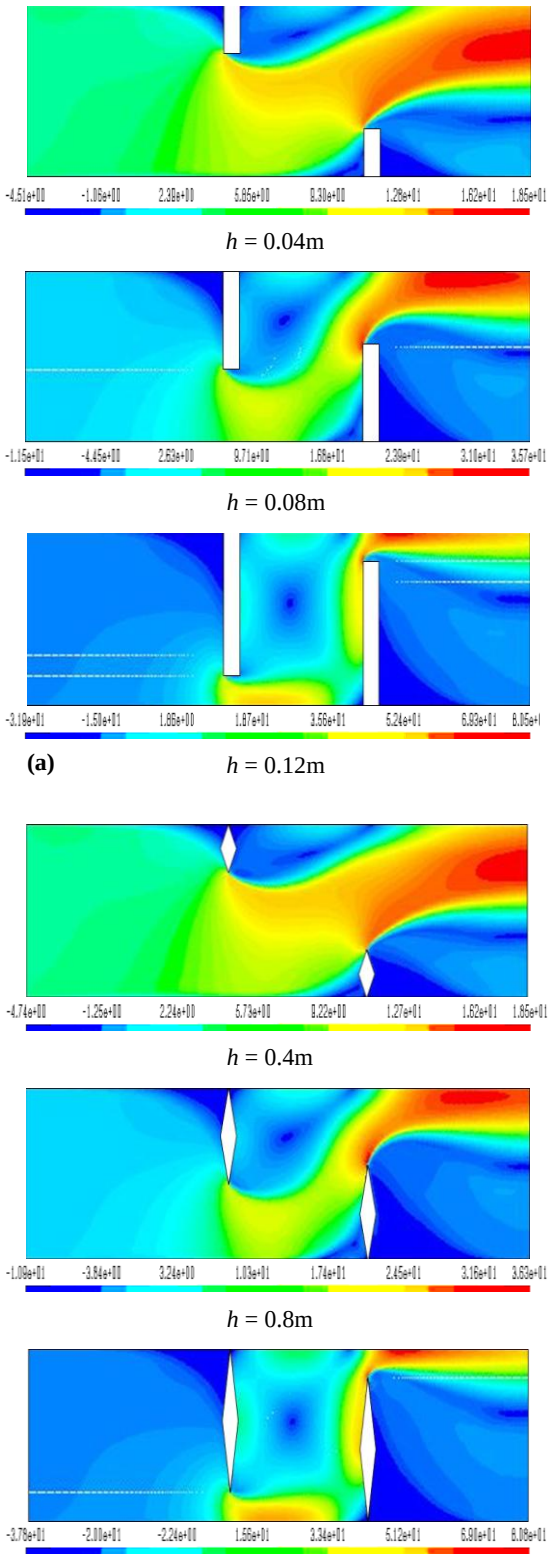

Figure 04: Effect of baffle height on velocity magnitude (unit: m/s) for: (a) flat and (b) diamond baffles, Re=8.73×10^4

3.2 Model Validation

In order to validate the studied approach and show the efficiency of proposed structured mesh, the studied numerical model is compared with the numerical and experimental model of Demartini et al. (2004) as shown in Figure 2. The plot shows our results and those obtained by Demartini et al. (2004). It represents the profiles of velocity at x = 0.525m. It is clear from Fig. 2 that the modeling results are in good agreement with the Demartini's experimental results. Even more importantly, it is concluded that the velocity profiles do not depend significantly on the shape of the baffle.

4 RESULTS AND DISCUSSION

The near wall flow structure in the presence of staggered baffles could be easily discerned by considering the streamline plots as depicted in Figures 3a and 3b for the cases of flat and diamond-shaped baffles, respectively. Here the streamlines around the baffle pair are presented for different baffle height values (h=0.04, 0.08, and 0.12 m) at Re=8.73×10^4. In all cases, a strong vortex is observed downstream of the baffle, which was induced due to the flow separation. The vortex was located close to the solid wall and its height was approximately equal to the extent of the flow blockage by the baffle, which is equal to 0.04 m, 0.08 m, and 0.12 m for the cases shown in Figure 3. This observation was confirmed by Nasiruddin and Kamran Siddiqui (2007).

The impact of the baffle height on the structure of the near wall flow is also depicted in Figure 4. The plots in Figure 4 show the velocity magnitudes for different baffle heights (h=0.04 m, h=0.08 m, and h=0.12 m at Re = 8.73×10^4. In the two treated cases, flat (Fig. 4a) and diamond (Fig. 4b) baffles, it is visible very low velocity values adjacent to the baffles. In the regions downstream of both baffles, recirculation cells with very low velocity values are observed as shown in Figure 3. In the regions between the tip of the baffles and the channel walls, the velocity is increased. Due to the changes in the flow direction produced by the baffles, the highest velocity values appear near the upper channel wall with an acceleration process that starts just after the second baffle, as indicated by Demartini et al. (2004). The results also show that the baffle height has an effect on the length of the recirculation zone and the magnitude of the maximum velocity.

The variation of velocity for the two cases appears clearly on the contours and their scales which present positive and negative values. For studying this dependence well, we plotted the velocity distribution at these sections: x=0.285 m, x=0.315 m and x=0.525 m, as shown in Figure 5a, b and c, respectively.

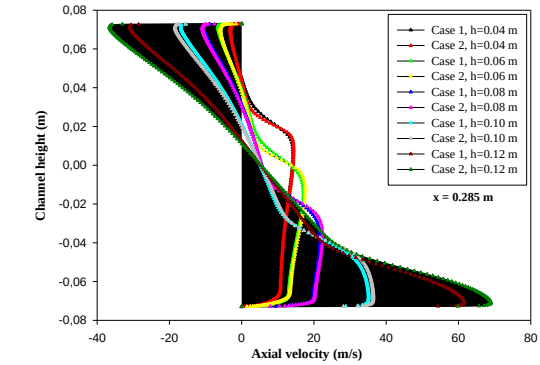

(a)

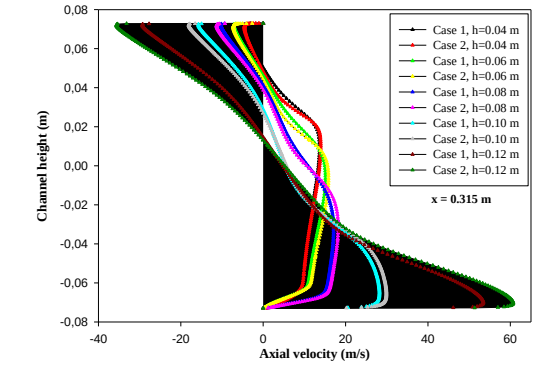

(b)

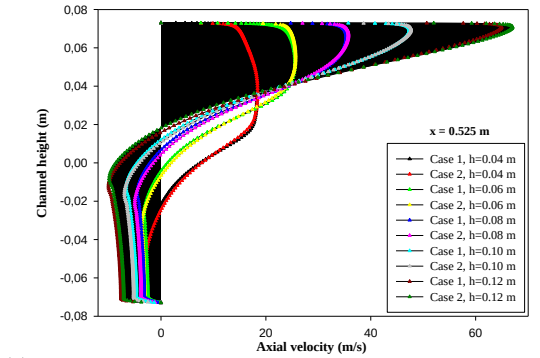

(c)

Figure 05: Variation of axial velocity profiles as a function of baffle height for the two treated cases (flat-shaped baffles: case 1, and diamond-shaped baffles: case 2) and: (a) Downstream of the top wall baffle, (b) upstream of the bottom wall baffle, and (c) near the channel outlet, Re=8.73×10^4

Figure 5a shows the variation of axial velocity profiles with various baffle height values (h=0.04 m, h=0.06 m, h=0.08 m, h=0.1 m and h=0.12m) at Re=8.73×10^4 in the position given by x=0.285 m, 0.057 m after the first baffle.

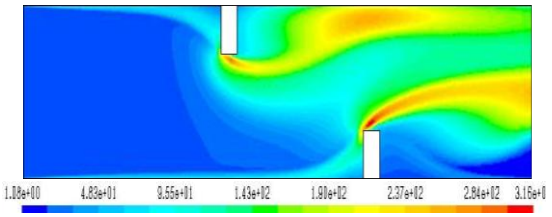

h = 0.04m

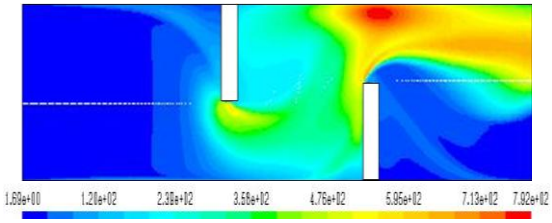

h = 0.08m

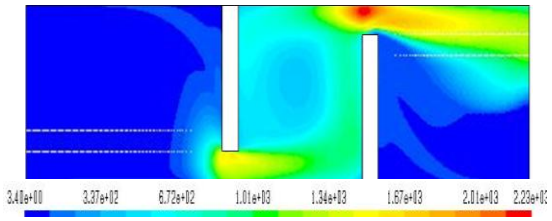

(a) *h* = 0.12m

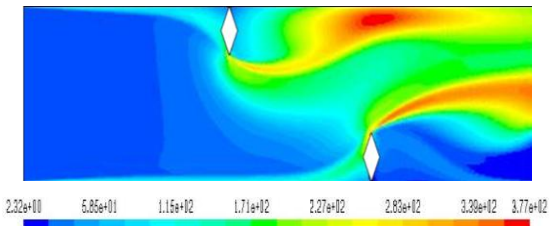

h = 0.04m

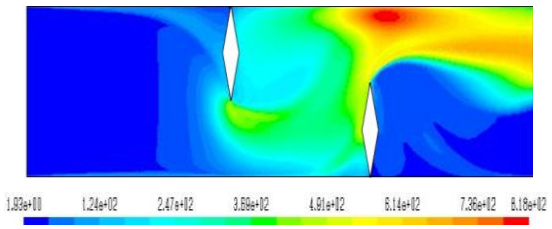

h = 0.08m

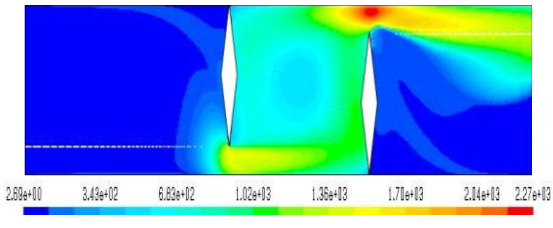

(b) *h* = 0.12m

Figure 06: Effect of baffle height on turbulent intensity (unit: %) for: (a) flat and (b) diamond baffles, Re=8.73×10^4

In the figure, it is visible that the flow downstream of the upper wall baffle is characterized by very high velocities at the lower part of the channel. In the upper part of the channel, negative velocities indicate the presence of recirculation behind the first baffle. Between the baffles, at the location x=0.315 m from entrance, 0.055 m before the bottom wall baffle, as the flow approaches the second baffle, its velocity is reduced in the lower part of the channel, while in the upper part is increased, as shown in Figure 5b. It is seen that the velocity profile is almost flat in the lower part of the channel, while in the upper part the flow starts to accelerate toward the gap above the second baffle. In that station, it is concluded that the influence of the deformation of the flow field increases as the flow approaches the second baffle, increasing the velocity of the flow approaching the passage above the baffle. A presentation of numerical results of axial velocity profiles after the bottom wall baffle, near the channel outlet, at a position x=0.525 m, 29 mm before channel outlet, is given in Figure 5c. The largest variations are found near the tip of the considered baffle. These values are only possible due to the very strong flow recirculation on the back side of the second baffle, which leads air from outside of the channel into the test section.

In all cases, as shown in Figure 5a, b and c, the maximum velocity is obtained for h=0.12 m while the lowest one is for h=0.04 m. Moreover, the magnitude of velocity increases for increasing the baffle height values, where the recirculation is strongly influenced by the height of the baffle, increasing when baffle height is increased, but remaining constant when the flow on the upper side of the baffle reattaches. What was also noticed, the use of diamond baffle (case 2) shows better velocity distribution values over the flat baffle (case 1) at all locations.

The contour plots of turbulent intensity are displayed in Figure 6a and b for the cases of flat and diamond baffles, respectively. The figure presents turbulent intensities of turbulent channel flow through baffles using h=0.04, 0.08, and 0.12 m. Here the turbulent intensity contours around the baffle pair are presented at Re=8.73×10^4. For all cases, the peak turbulence intensity values, predicted by the k-ε turbulence model, are seen on the top of baffle front regions, while the turbulence intensity is observed to be very low at baffle bottom wall area. A large turbulence intensity zone is found in the regions between the tip of the baffle and the channel walls close to the main flow which yields the strong influence of turbulence intensity on heat transfer enhancement.

Figure 7a and b displays the variation of the average Nusselt number and friction factor with different baffle height values at the surface of lower (y=-H/2) and upper (y=H/2) channel walls and two various examined baffle shape geometries (flat baffles: case 1, and diamond baffles: case 2), respectively.

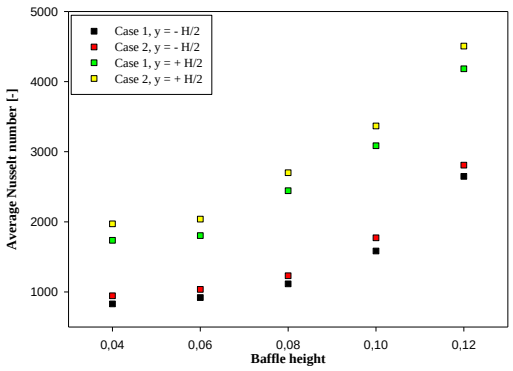

(a)

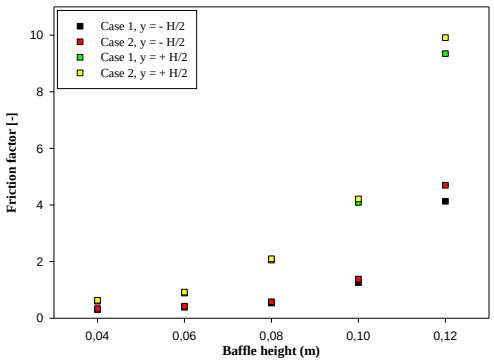

(b)

Figure 07: Effect of (a) Average Nusselt number and (b) friction factor, with baffle height at the surface of lower and upper channel walls for two various investigated baffle shape cases (flat-shaped: case 1, and diamond-shaped: case 2), Re=8.73×10^4

In all cases, flat and/or diamond baffles, it is noted that both the average Nusselt number and friction factor values tend to increase with the rise of baffle height values. This can be attributed to the fact that increasing the rib height can induce a larger recirculation zone behind the rib leading to higher vortex (recirculation/reverse flow) strength and turbulence intensity of the flow, enhancing the heat transfer and pressure drop. In addition, the baffle with h=0.12 m gives the highest Nusselt number and friction factor while the one with h=0.04 m provides the lowest.

The slope of $\overline{Nu}$ and f curves increases for high h values and the highest Nusselt number and friction factor is obtained when the channel wall is y=H/2 (top channel wall) in which there is more flow resistance. In that heated station, the $\overline{Nu}$ and f values for the duct with diamond-shaped baffles (case 2) appear to be about 0,915-1,077 and 1,041-1,175 times above those for the duct with flat-shaped baffles, depending on the h values.

5 CONCLUSION

In this present analysis, a numerical prediction has been conducted to study heat transfer and flow friction behaviors in turbulent channel flows over staggered baffles of different heights. Five baffle height values (h=0.04, 0.06, 0.08, 0.1 and 0.12 m) were designed for computational investigation, and a comparison with differently shaped baffles (e.g. flat rectangular and diamond) was also carried out. The validation of the flow structure of the baffled channel was performed by comparing with the previous research under similar conditions. The flow structure is affected by the presence of these baffles, resulting in the formation of recirculation cells downstream from each baffle. The most intense is that occurring downstream of the bottom wall baffle (second baffle), responsible for the high flow velocities observed at the channel outlet, creating a negative velocity profile which introduces mass inside the computational domain through the outlet. This observation is confirmed by Demartini et al. (2004). The size of theses recirculation zones strongly depend on the solid baffle properties (shape and height). This flow structure has profound influences on the heat transfer characteristics. The variation of average Nusselt number is presented in this research which shows that the Nusselt number increases with the rise of baffle height values. In all cases, the channel flows with diamond-shaped baffles give higher values of Nusselt number than that for channel flow with baffle plates (flat-shaped baffles) due to the induction of high recirculation/reverse flow and thin boundary layer, increasing turbulence levels, leading to higher temperature gradients. Also, inserting shaped solid baffles has the effect of increasing the pressure drop in the channel. This augmentation is more important at high baffle height and for the diamond shape.

NOMENCLATURE

$C_{1\varepsilon}$	constant used in the standard *k-ε* model
$C_{2\varepsilon}$	constant used in the standard *k-ε* model
$C_{3\varepsilon}$	constant used in the standard *k-ε* model
D_h	channel hydraulic diameter, m
f	friction factor
G_k	production of turbulent kinetic energy, m^2/s^2
H	channel height, m
h	baffle height, m
h_x	local convective heat transfer coefficient, $W.m^{-2}.K^{-1}$
k	turbulent kinetic energy, m^2/s^2
L	Length of rectangular channel in *x*-direction, m
L_1	distance upstream of the first baffle, m
L_2	distance downstream of the second baffle, m
$\overline{Nu}$	Average Nusselt number
ΔP	pressure drop, Pa
P	pressure, Pa
Pi	baffle distance or spacing, m
P_{atm}	atmospheric pressure, Pa
Re	Reynolds number
S_ϕ	source term
T	temperature, °C
T_{in}	inlet temperature, °C
T_w	wall temperature, °C
$\overline{U}$	mean axial velocity of the section, m/s
U_{in}	inlet velocity, m/s
u	fluid velocity in x-direction, m/s
v	fluid velocity in y-direction, m/s
w	baffle width, m
x	Cartesian coordinate in x-direction, m
y	Cartesian coordinate in y-direction, m

Greek symbols

ε	specific dissipation rate, m^2/s^2
Γ_ϕ	diffusion coefficient, Kg/m.s
ρ	fluid density, Kg/m^3
ν	Kinematics viscosity, m^2/s
μ	molecular viscosity, Kg/m.s
μ_l	laminar viscosity, Kg/m.s
μt	eddy viscosity, Kg/m.s
σ_k	turbulent Prandtl number for k-equation
σ_ε	turbulent Prandtl number for ε-equation
λ_f	fluid thermal conductivity,W/m.°C
ϕ	stands for the dependent variables u, v, k, ε, and T

Subscript

atm	atmospheric
f	fluid
in	inlet of the computational domain
s	solid
t	turbulent
w	wall
x	local

REFERENCES

[1] Demartini L.C., Vielmo H.A. and Möller S.V., 2004. Numerical and experimental analysis of the turbulent flow through a channel with plate baffles. Journal of Braz. Soc. Of Mech. Sci. & Eng., 26(2), 153-159.

[2] Endres L.A.M. and Möller S.V., 2001. On the fluctuating wall pressure field in tube banks. Nuclear Engineering & Design, 203, 13-26.

[3] Fluent Inc., 2006. User´s Guide 6.3. Centerra Park Lebanon, NH, USA.

[4] Kang-Hoon K. and Anand N.K., 2003. Use of porous baffles to enhance heat transfer in a rectangular channel. Int. J. Heat and Mass Transfer, 46(22), 4191-4199.

[5] Karwa R. and Maheshwari B.K., 2009. Heat transfer and friction in an asymmetrically heated rectangular duct with half and fully perforated baffles at different pitches. Int. Comm. Heat and Mass Transfer 32(3), 264-268.

[6] Karwa R., Maheshwari B.K. and Karwa N., 2005. Experimental study of heat transfer enhancement in an asymmetrically heated rectangular duct with perforated baffles. Int. Comm. Heat and Mass Transfer, 32(1-2), 275-284.

[7] Launder B.E. and Spalding D.B., 1974. The Numerical computation of Turbulent Flows. Computer Methods in Applied Mech. and Eng. 3, 269-289.

[8] Lei Y.G., He Y.L., Chu P. and Li R., 2008. Design and optimization of heat exchangers with helical baffles. Chemical Eng. Science, 63(17), 4386-4395.

[9] Molki M. and Mostoufizadeh A.R., 1989. Turbulent heat transfer in rectangular ducts with repeated-baffle blockages. Int. J. Heat and Mass Transfer, 32, 491-1499.

[10] Nasiruddin and Siddiqui Kamran M.H., 2007. Heat transfer augmentation in a heat exchanger tub using a baffle. Int. J. Heat and Fluid Flow, 28(2), 318-328.

[11] Patankar S.V., 1980. Numerical heat transfer and fluid flow, McGraw-Hill, New York.

[12] Tandiroglu A., 2006. Effect of flow geometry parameters on transient heat transfer for turbulent flow in a circular tube with baffle inserts. Int. J. Heat and Mass Transfer 49, 1559-1567.

[13] Wilfried R. and Deiying W.L., 1994. Effect of baffle/shell leakage flow on heat transfer in shell-and-tube heat exchanger. Experimental Thermal and Fluid Science, 8(1), 10-20.